ChemComm

COMMUNICATION

View Article Online
View Journal | View Issue

Cite this: *Chem. Commun.*, 2024, **60**, 4805

Received 3rd March 2024,
Accepted 4th April 2024

DOI: 10.1039/d4cc01017e

rsc.li/chemcomm

A rapid and eco-friendly approach for the synthesis of low-silica SAPO-34 with excellent MTO catalytic performance†

Xiaoxia Zou,[ab] Dong Fan,[b] Xiaosi Zhang,[bc] Caiyi Lou,[bc] Miao Yang,[b] Shutao Xu,[b] Quanyi Wang,*[b] Peng Tian*[b] and Zhongmin Liu[bc]

A rapid and eco-friendly route has been developed for the synthesis of SAPO-34 with short crystallization time (1–3 h), low silica content (as low as 6.2 wt%) and excellent methanol-to-olefin (MTO) catalytic performance by utilization of a recycled mother liquid at elevated crystallization temperature.

The methanol-to-olefin (MTO) process is a pivotal technology in the C1 chemistry industry, as it provides a non-petrol route for the production of ethene and propene.[1–4] A SAPO-34 molecular sieve with the isomorphic structure of zeolite chabazite (CHA) is hitherto the most effective component for MTO catalysts and has been attracting significant interest from both academia and industry. The CHA structure of SAPO-34 is fabricated by the ordered arrangements of double 6-membered rings, forming barrel-like nanocages featuring 8-membered ring openings. This special structure provides an ideal "incubation cradle" for the development of polymethylbezene species, the authentic active center for the MTO reaction.[3] Commercial MTO utility with an olefin production capacity of 600 000 tons was first commissioned in 2010. Since then, an emerging MTO industry has been booming in China with the olefin production capacity reaching 17 million tons per annum.[5]

With the booming of the MTO industry, the annual demand for SAPO-34 based catalysts has now increased up to 10 000 tons. Conventionally, SAPO-34 is synthesized *via* a hydrothermal route. One drawback associated with the hydrothermal production of SAPO-34 is the co-production of large quantities of a mother liquid, commonly regarded as industrial waste and demanding expensive disposals to meet environmental regulations. The discharge of a mother liquid not only results in a waste of unreacted raw resources but also intrigues serious environmental problems. It is highly valuable to develop an effective method to convert the mother liquid into an efficient SAPO-34 catalyst. Moreover, it has been recognized that SAPO-34 with low silica content (low acid density) can restrain side reactions and lead to enhanced MTO performance,[6] which implies the importance of controlling the low silica content of SAPO-34, when attempting to convert the mother liquid into SAPO-34. This is indeed a challenging work, as previous works demonstrated that low-silica SAPO-34 products were easily contaminated by impurities (SAPO-5, -11, *etc.*) or intergrown with an AEI phase,[6,7] causing a reduced ethene plus propene selectivity.[8] In addition, Yu *et al.* once reported a breakthrough in synthesizing hierarchical SAPO-34 through recycling the mother liquid and incorporating HF, albeit with low solid yields (34%).[9] Yan *et al.* demonstrated that SAPO-34 can be synthesized using the mother liquid as the seed, effectively reducing the template dosage.[10]

In the present study, an eco-friendly approach with the utilization of the recycled mother liquid was reported for the synthesis of SAPO-34. The developed system can allow an elevated crystallization temperature, leading to fast synthesis of SAPO-34 within 1–3 h and with reduced silica content. Both the product phase and crystallization kinetics were demonstrated to be significantly dependent on the crystallization temperature and the dosage of the mother liquid. The rapidly synthesized low-silica SAPO-34 was well characterized and its MTO catalytic performance was evaluated.

To gain a comprehensive understanding of the composition and properties of the recycled mother liquid, detailed characterization studies were carried out and the results are illustrated in Fig. S1 (ESI†). The solid content of the mother liquid was measured to be around 16.9 wt%, where SiO_2, Al_2O_3 and P_2O_5 account for 0.46 wt%, 6.69 wt% and 9.70 wt%,

[a] *Henan Institute of Advanced Technology, Zhengzhou University, Zhengzhou 450003, China*
[b] *National Engineering Research Center of Lower-Carbon Catalysis Technology, Dalian National Laboratory for Clean Energy, Dalian Institute of Chemical Physics, Chinese Academy of Sciences, Dalian 116023, China. E-mail: qywang@dicp.ac.cn, tianpeng@dicp.ac.cn*
[c] *University of Chinese Academy of Sciences, Chinese Academy of Sciences, Beijing 100049, China*

† Electronic supplementary information (ESI) available. See DOI: https://doi.org/10.1039/d4cc01017e

Table 1 Synthesis of the samples with different templates by the utilization of the recycled mother liquid

		Product		
Sample[a]	x R	Crystal phase	Yield (wt%)	Elemental composition
1	3.0 MOR	CHA + minor AEL	70.1	$Al_{0.497}P_{0.423}Si_{0.079}O_2$
2	2.0 DEA	CHA	53.1	$Al_{0.500}P_{0.405}Si_{0.096}O_2$
3	2.0 TEAOH	CHA	49.6	$Al_{0.504}P_{0.406}Si_{0.090}O_2$
4	3.0 TEA	CHA/AEI	88.1	$Al_{0.492}P_{0.446}Si_{0.062}O_2$
5	1.0 TEA/2.0 DEA	CHA	62.3	$Al_{0.503}P_{0.410}Si_{0.087}O_2$
6	1.5 TEA/1.5 DEA	CHA	68.0	$Al_{0.502}P_{0.421}Si_{0.078}O_2$
7[b]	2.0 TEA/1.0 DEA	CHA	81.0	$Al_{0.501}P_{0.425}Si_{0.074}O_2$
$1_{Ref.}$[b,c]	2.0 TEA/1.0 DEA	CHA/AEI + minor AFI	74.8	$Al_{0.501}P_{0.429}Si_{0.069}O_2$
$2_{Ref.}$[c,d]	2.0 TEA/1.0 DEA	CHA	53.4	$Al_{0.503}P_{0.421}Si_{0.076}O_2$

[a] The gel molar composition was 1.0 Al_2O_3 : 1.0 P_2O_5 : 0.25 SiO_2 : x R : 50 H_2O (220 °C, 5 h, 40 g of the mother liquid). M1/M2 = 52.2 wt%, where M1 and M2 were dry oxides from the mother liquid and the final gel, respectively. [b] The crystallization was at 220 °C for 3 h. [c] Without the addition of the mother liquid. [d] The synthesis for $2_{Ref.}$ was with 0.20 SiO_2 in the gel at 200 °C for 12 h.

respectively. The diluted mother liquid was detected by DLS measurements, revealing the existence of small colloid particles with a mean size of about 19 nm. After drying and calcination, the solid residues of the mother liquid exhibit no detectable SAPO-34 phase in the XRD patterns. ^{29}Si, ^{31}P and ^{27}Al NMR spectra were further measured to probe the atomic coordination environments of the mother liquid. Their detailed assignments are given in Fig. S1 (ESI†), which demonstrate that the environments of Si and Al atoms are highly diverse and heterogeneous, whereas the status of P atoms appears relatively uniform in the mother liquid.

It is well-known that organotemplates play a crucial role in the crystallization of molecular sieves, influencing both the crystal phases and morphologies of the products. In this study, four common templates for SAPO-34 synthesis, including morpholine (MOR), tetraethylammonium hydroxide (TEAOH), diethylamine (DEA) and triethylamine (TEA), were initially trialed for rapid synthesis with the presence of the mother liquid. The detailed synthesis protocols and results are shown in Table 1 and Fig. S2 (ESI†). Under the investigated conditions (220 °C), employing MOR as the template resulted in a product mixture of CHA and minor AEL (sample 1), which is likely caused by the lower SiO_2 dosage and higher crystallization temperature. SAPO-34 (samples 2 and 3) could be readily synthesized using DEA or TEAOH as the template. However, obviously low yields (*ca.* 50%) and elevated silica contents were observed for both samples, which are speculated to be related to the stronger alkalinity associated with DEA and TEAOH.[11,12] When using TEA as the template (sample 4), the solid yield was significantly increased to 88.1%, suggesting a better raw source utilization efficiency. However, the product has an intergrowth phase of CHA/AEI, instead of the pure CHA phase. This is not surprising as AEI intergrowth is the common concomitant phase in conventional synthesis using the TEA template.[13]

A dual template system based on TEA and DEA was further designed, with the expectation that the addition of DEA can help restrain the formation of AEI intergrown. As shown in Table 1 and Fig. S3 (ESI†), three synthesis batches with varying TEA/DEA ratios were carried out, and they all delivered pure SAPO-34 as the final product. This clearly demonstrates the potent effect of DEA in restraining the AEI intergrown, probably due to its strong structure-directing ability towards the CHA structure.[11] With the increase of TEA/DEA ratios, the product featured with a decreased silica content, accompanied by a concomitant increase of solid yields. All these samples possess the rhombohedral morphology typical for SAPO-34. Samples 5 and 6 crystallized under relatively high DEA concentrations exhibit a comparatively large crystal size (*ca.* 5 μm), while for sample 7 the crystal size decreases to *ca.* 2 μm. A control experiment (sample $1_{Ref.}$, Fig. S4, ESI†) was further designed, employing the same method as that of sample 7, except exclusively utilizing fresh raw sources. A CHA/AEI intergrowth accompanied by a small amount of AFI impurity became the final product (*ca.* 10 μm). This implies that the addition of the mother liquid can help in suppressing the formation of intergrown/impurity and effectively reduce the crystal sizes of SAPO-34.

The impact of crystallization temperatures on SAPO-34 synthesis was investigated based on the gel system of sample 7. As evidenced by the XRD patterns in Fig. S5 (ESI†), all five samples exhibit diffraction peaks characteristic of CHA topology after 3 h crystallization at varying temperatures from 200 to 240 °C. SEM images reveal that the samples have the rhombohedral morphology, and the sample crystallized at 240 °C possesses obviously small crystal sizes. Moreover, it is noted that a small amount of amorphous impurities can be observed in the SEM image of the sample synthesized at 200 °C, suggesting its slower crystallization rate.

A systematic investigation of the crystallization kinetics is carried out to gain a deeper understanding of the crystallization behaviors at different temperatures. The evolution of relative crystallinity and solid yields of the products is illustrated in Fig. 1. As expected, a relatively slow crystallization is observed for the sample synthesized at 200 °C. No crystalline product could be collected after a crystallization duration of 1 h. Afterward, a small quantity of SAPO-34 can be formed, albeit with low crystallinity. The relative crystallinity rose gradually, reaching full crystallinity at 4 h. Its slow crystallization is also evidenced by its distinct variation trend in solid yields. The yield for the collected solids rises slowly and reaches a maximum value of 74% after 8 h. With the elevation of temperature, the crystallization accelerates significantly. The most striking outcome is observed for the samples crystallized at 240 °C, achieving a relative crystallinity of 87% after crystallization for

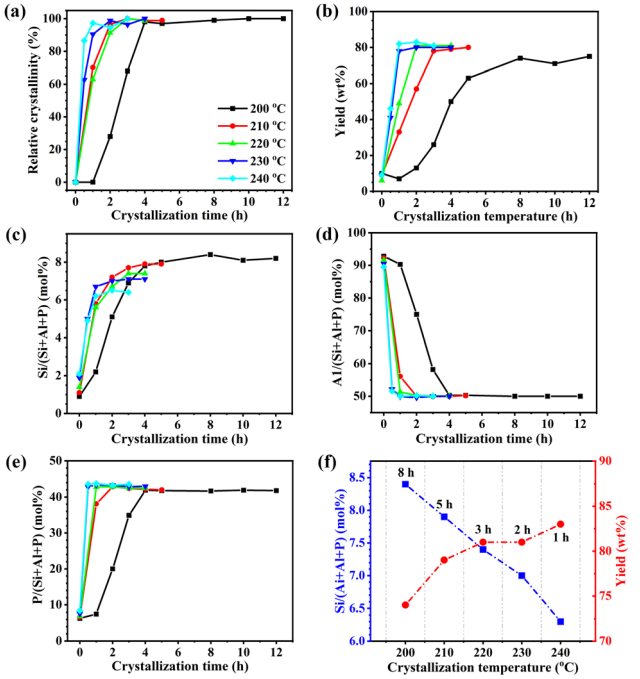

Fig. 1 The evolution of (a) relative crystallinity, (b) solid yields and (c)–(e) product inorganic elemental compositions during the synthesis of SAPO-34 at different temperatures (based on the gel system of sample 7). (f) Comparison of solid yields and product silica contents. The data in (f) were the equilibrium values at each crystallization temperature. The corresponding crystallization times of the data were labelled in (f).

merely 0.5 h and almost 100% at 1 h (named sample 8). Simultaneously, the solid yield reaches a maximum value of 83% at 1 h. Fig. S6 (ESI†) gives the characterization results of sample 8, evidencing its purity and high crystallinity.

The evolution of inorganic elemental compositions of the samples is given in Fig. 1c–e. For the initial 0 h solids, the Al_2O_3 contents are dominant. Subsequently, the contents of SiO_2 and P_2O_5 in the solids increase significantly together with the decrease of the Al_2O_3 content, suggesting that Si and P atoms participate in the formation of the SAPO-34 framework from the liquid phase. Following the proceeding of crystallization, the P_2O_5 and Al_2O_3 contents of the products approach equilibrium values, in agreement with the obviously increased crystallinity. The SiO_2 contents always keep an increasing trend, even after the relative crystallinity of the solids reaches about 100%. This phenomenon is consistent with our previous investigation on SAPO-34 synthesis using conventional raw sources at 200 °C, which implies an increased Si content from the core to the shell of the crystals.[14,15] This should be caused by the relatively low reactivity of Si sources than that of Al and P sources.

Fig. 1f compares the equilibrium Si contents and solid yields at different crystallization temperatures. The two curves present opposite trends, indicating that elevating the crystallization temperature can enhance solid yields, but inhibit the incorporation of Si into the framework of SAPO-34. At 240 °C, the product possesses the lowest silica content of 6.2 wt% together with a maximum yield (83%) after crystallization of only 1 h. These results demonstrate the powerful effect of mother liquid assistance on the synthesis of low-silica SAPO-34 at elevated temperatures. As the templates can be easily distilled out and recycled after synthesis,[15] this system provides an eco-friendly and sustainable approach for the synthesis of SAPO-34.

Synthesis trials with varying mother liquid amounts based on the TEA-DEA system were further carried out to study the effect of mother liquid addition. The results are shown in Table S1 and Fig. S7 (ESI†). In the absence of the mother liquid, the product is SAPO-34/SAPO-18 intergrown together with small amounts of SAPO-5 impurities, similar to that observed for sample 1_{Ref}. Following the increased addition of the mother liquid, the products become pure SAPO-34 with relatively small crystal sizes and the solid yields show a gradual increase from the initial 40.1% to 78–80%. These results imply that the addition of the mother liquid can help in restraining the intergrowth and impurity and promote the fast nucleation and crystallization of SAPO-34. The synthesis results with the assistance of seed are given in Table S1 and Fig. S8 (ESI†). The product (sample $3_{Ref.}$) is a SAPO-34/SAPO-18 intergrown but without the SAPO-5 impurity and has a high solid yield of 79%. It is thus speculated that there may exist microscopic structure units of SAPO-34 in the mother liquid, which can effectively restrain impurity and enhance the crystallization rate of SAPO-34.

Table S2 (ESI†) lists the variation of the product phase, solid yield and silica content with the change of initial SiO_2 dosage based on the TEA-DEA system. The corresponding XRD patterns and SEM images of the products are shown in Fig. S9 (ESI†). Under the investigated conditions (at 230 °C for 2 h), when the initial $x(SiO_2)$ is 0.10 or 0.15, SAPO-34 with a small amount of SAPO-5 impurity was obtained. Increasing $x(SiO_2)$ to 0.15 or higher leads to the crystallization of pure SAPO-34. The solid yield and product silica content rise with the incremental SiO_2 dosage, whereas the Si incorporation degree shows a declining trend.

Fig. S10 (ESI†) displays the crystallization kinetics of the samples with different initial silica dosages. The relative crystallinity, solid yield and silica content of all four systems present a sharp increase in the first 1 h. The relative crystallinity of the 1 h samples reaches 90% or higher, and the corresponding yields are also close to the final values. It is interesting to note that high silica systems possess relatively fast crystallization rates, implying that the hydrolysis and reaction of Si sources are critical for nucleation and growth of SAPO-34.

The textural properties of the rapidly synthesized low-silica SAPO-34 (samples 7, 8 and 15), crystallized at different temperatures, were evaluated by N_2 sorption analysis. As listed in Table S3 (ESI†), the micropore surface areas range from 530 to 560 $m^2\ g^{-1}$ among the samples, while the micropore volume is 0.26 $cm^3\ g^{-1}$, suggesting the good crystallinity of the samples. The ^{29}Si, ^{27}Al and ^{31}P MAS NMR spectra are recorded to probe the local coordination environments in the as-synthesized SAPO-34 samples (Fig. 2). A single resonance band centered at around −28.5 ppm is observed in the ^{31}P spectra for all the samples, suggesting that the P species are in the tetra-

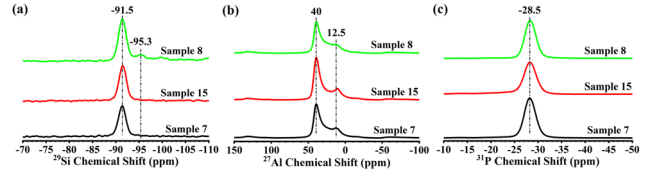

Fig. 2 (a) ^{29}Si, (b) ^{27}Al and (c) ^{31}P MAS NMR spectra of the as-synthesized SAPO-34.

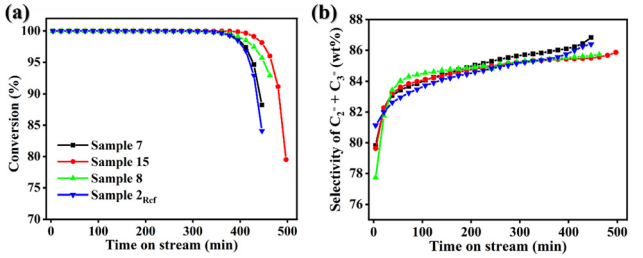

Fig. 3 (a) Methanol conversion and (b) selectivity of ethene plus propene with time on stream over samples. Reaction conditions: $WHSV_{methanol}$ = 2.0 h^{-1}, T = 450 °C.

coordinated form in the framework.[16] In the ^{27}Al spectra, two resonance bands could be observed. The predominant band at around 40 ppm corresponds to the tetra-coordinated framework Al, while the shoulder at around 12.5 ppm is due to penta-coordinated Al, which is speculated to be due to its coordination with an extra template or a water molecule.[17] The ^{29}Si MAS NMR spectra exhibit a sole resonance band centered around −91.5 ppm for samples 7 and 15, indicating that Si atoms exist exclusively in the Si(^{4}Al) environment in both samples. For sample 8 synthesized at 240 °C for 1 h, a small resonance at −95.3 ppm can also be discerned, which is ascribed to the Si(^{3}Al)(^{1}Si) species on the rim of Si islands.[18] The existence of Si islands was further confirmed by the ^{29}Si MAS NMR spectrum of the sample crystallized at 240 °C for 3 h (Fig. S11, ESI†). Considering the low silica content of sample 8, the occurrence of Si islands might be due to the surface Si enrichment associated with high crystallization temperatures.

The surface elemental compositions of the samples were further determined using XPS. From Table 2, a surface Si enrichment phenomenon was observed for all the investigated samples. The surface Si enrichment degree is more evident for the samples with higher SiO_2 contents (samples 16 and 17). This again confirms that the relatively low reactivity of silica sources led to the formation of a Si- deficient core at the early crystallization stage. For sample 8, its surface Si content is lower than those of samples 7 and 15. The occurrence of Si islands on sample 8 is speculated to be caused by its subtle microstructural variations arising from the higher crystallization temperature. More likely, there may exist small amounts of CHA/AEI intergrowth (lower than the detection limit of the XRD measurement) in sample 8, given that Si islands can be easily formed in low-silica SAPO-18.[19] Moreover, samples 18 and $2_{Ref.}$ show comparable surface Si enrichment degrees. As both samples were synthesized at the same temperature using the mother liquid and conventional sources respectively, it is speculated that the use of the mother liquid has little impact on the Si incorporation, likely owing to the low silica content of the mother liquid.

NH_3-TPD was employed to probe the acid properties of the rapidly synthesized low-silica SAPO-34 (samples 7, 8 and 15). From Fig. S12 (ESI†), the high-temperature desorption band corresponds to the acid sites with medium/high acid strength, while the low-temperature peak is due to NH_3 desorption from the weak acid sites. The NH_3-TPD curves are almost identical for samples 7 and 15, indicating the similar acid properties of both samples. In contrast, sample 8 exhibits a relatively low acid amount, in congruence with its low silica content and partially due to the formation of Si islands.

The MTO catalytic performance of the rapidly synthesized low-silica SAPO-34 was evaluated and is displayed in Fig. 3 and Table S4 (ESI†). Under the investigated conditions, all samples displayed a comparable long catalytic lifetime (378–420 min) and high selectivity towards ethene and propene. The highest selectivity on the samples reaches 85.5–86.0 wt% (>99% methanol conversion), which is at the top level among MTO catalysts.[6] Interestingly, despite the presence of trace amounts of Si islands within sample 8, its catalytic lifetime and the highest selectivity of ethene and propene were not compromised. This is speculated to be related to its low silica content and consequently low acid concentrations as revealed by NH_3-TPD. A reference sample ($2_{Ref.}$, Table 1 and Fig. S4, ESI†) with a comparative low-silica content, prepared based on conventional sources and conditions, was also evaluated for comparison. Its catalytic lifetime and selectivity of light olefines are

Table 2 Elemental compositions of the rapidly synthesized SAPO-34

		Elemental compositions (in mole)		
Sample	T-time[a]	XRF	XPS	Si_{XPS}/Si_{XRF}
7	220 °C-3 h	$Al_{0.501}P_{0.425}Si_{0.074}O_2$	$Al_{0.497}P_{0.391}Si_{0.111}O_2$	1.50
15	230 °C-2 h	$Al_{0.500}P_{0.433}Si_{0.070}O_2$	$Al_{0.487}P_{0.383}Si_{0.130}O_2$	1.86
8	240 °C-1 h	$Al_{0.506}P_{0.431}Si_{0.063}O_2$	$A1_{0.500}P_{0.408}Si_{0.092}O_2$	1.46
18	200 °C-10 h	$Al_{0.500}P_{0.419}Si_{0.080}O_2$	$Al_{0.499}P_{0.388}Si_{0.113}O_2$	1.41
16	230 °C-2 h	$Al_{0.499}P_{0.420}Si_{0.081}O_2$	$A1_{0.453}P_{0.331}Si_{0.216}O_2$	2.67
17	230 °C-2 h	$Al_{0.494}P_{0.419}Si_{0.088}O_2$	$Al_{0.456}P_{0.353}Si_{0.191}O_2$	2.17
$2_{Ref.}$	200 °C-12 h	$Al_{0.503}P_{0.421}Si_{0.076}O_2$	$Al_{0.492}P_{0.406}Si_{0.103}O_2$	1.36

[a] T and time were the crystallization temperature and time, respectively.

comparable with those of samples 7, 8 and 15, evidencing the good MTO catalytic performance of the rapidly synthesized SAPO-34 assisted by the recycled mother liquid.

In summary, a rapid and eco-friendly route has been developed for the synthesis of low-silica SAPO-34 by the utilization of the mother liquid and dual template (TEA and DEA) at elevated crystallization temperatures. The addition of the mother liquid can effectively restrain the impurity/intergrowth and fasten the crystallization of SAPO-34, likely owing to the microscopic structure units of SAPO-34 in the mother liquid. The low-silica samples exhibited good MTO catalytic performance due to their high crystallinity and suitable acid properties. This study holds potential to contribute to the more efficient and cost-effective manufacture of industrial MTO catalysts.

This work is supported by the National Natural Science Foundation of China (No. 22288101, 21991090, 21991091, 22171259, and 22272173) and the AIS&T Program of Yulin Branch, Dalian National Laboratory for Clean Energy, CAS (DNL-YL A202206). The authors are grateful for the funding from the Sino-French IRN (International Research Network).

Conflicts of interest

There are no conflicts to declare.

Notes and references

1 Y. Irina, C. Dutta, M. Florian, B. Weckhuysen and G. Jorge, *Nat. Catal.*, 2018, **1**, 398–411.
2 U. Olsbye, S. Svelle, M. Bjørgen, P. Beato, T. Janssens, F. Joensen, S. Bordiga and K. Lillerud, *Angew. Chem., Int. Ed.*, 2012, **51**, 5810–5831.
3 W. Zhang, S. Lin, Y. Wei, P. Tian, M. Ye and Z. Liu, *Natl. Sci. Rev.*, 2023, nwad120.
4 Q. Sun, Z. Xie and J. Yu, *Natl. Sci. Rev.*, 2018, **5**, 542–558.
5 Z. Liu, Q. Wang, S. Liu, M. Yang, D. Fan, D. Zhu and P. Tian, *Mater. Today Sustainable*, 2023, **21**, 100302.
6 M. Yang, D. Fan, Y. Wei, P. Tian and Z. Liu, *Adv. Mater.*, 2019, **31**, 1902181.
7 B. Gao, M. Yang, Y. Qiao, J. Li, X. Xiang, P. Wu, Y. Wei, S. Xu, P. Tian and Z. Liu, *Catal. Sci. Technol.*, 2016, **6**, 7569–7578.
8 P. Wu, M. Yang, L. Sun, S. Zeng, S. Xu, P. Tian and Z. Liu, *Chem. Commun.*, 2018, **54**, 11160–11163.
9 D. Xi, Q. Sun, X. Chen, N. Wang and J. Yu, *Chem. Commun.*, 2015, **51**, 11987–11989.
10 Z. Liu, H. Li, T. Zhang, Y. Wang, P. Shi, Y. Wang, F. Subhan, X. Liu and Z. Yan, *Catal. Today*, 2020, **358**, 109–115.
11 G. Liu, P. Tian, J. Li, D. Zhang, F. Zhou and Z. Liu, *Microporous Mesoporous Mater.*, 2008, **111**, 143–149.
12 Y. Cao, D. Fan, D. Zhu, L. Sun, L. Cao, P. Tian and Z. Liu, *J. Catal.*, 2020, **391**, 404–413.
13 B. Shen, X. Chen, X. Fan, H. Xiong, H. Wang, W. Qian, Y. Wang and F. Wei, *Nat. Commun.*, 2021, **12**, 2212.
14 G. Liu, P. Tian, Y. Zhang, J. Li, L. Xu, S. Meng and Z. Liu, *Microporous Mesoporous Mater.*, 2008, **114**, 416–423.
15 P. Tian, Y. Wei, M. Ye and Z. Liu, *ACS Catal.*, 2015, **5**, 1922–1938.
16 Y. Huang, D. Machado and C. W. Kirby, *J. Phys. Chem. B*, 2004, **108**, 1855–1865.
17 C. S. Blackwell and R. L. Patton, *J. Phys. Chem.*, 1988, **92**, 3965–3970.
18 S. Ashtekar, S. V. Chilukuri and D. K. Chakrabarty, *J. Phys. Chem.*, 1994, **98**, 4878–4883.
19 J. Chen, P. A. Wright, J. M. Thomas, S. Natarajan, L. Marchese, S. M. Bradley, G. Sankar and C. R. A. Catlow, *J. Phys. Chem.*, 1994, **98**, 10216–10224.